Hot electrons in wurtzite indium nitride

N. A. Masyukov and A. V. Dmitriev[a)]
The Faculty of Physics, Moscow State University, Moscow 119991, Russia

(Received 19 November 2010; accepted 1 December 2010; published online 19 January 2011)

In this paper we study hot electron transport in bulk wurtzite *n*-InN using an iterative numerical method. We calculate field dependence of the electron drift velocity using several sets of the material parameters that can be found in the literature, and the results are compared with the available experimental data. Then, we perform more detailed calculations for different lattice temperatures and different carrier concentrations using the material parameters that provide the best fit to the experimental data. © *2011 American Institute of Physics*. [doi:10.1063/1.3533981]

I. INTRODUCTION

For a long time, the band gap width of around 2 eV was assumed in the wurtzite InN. However, recent experimental and theoretical studies have provided convincing evidence that the band gap in InN is actually close to 0.7 eV.[1,2] Thus, the alloys $In_xGa_{1-x}N$ of InN with wideband GaN can be widely used in optoelectronic applications, particularly in general light sources.[3] So electrical properties of these materials attract much interest, and the problem of charge transport in these semiconductors in high electric fields becomes more important.

The charge carrier transport in the nitride semiconductors has been studied theoretically many times in recent years. For example, hot-electron transport in InN was studied numerically in papers[4–10] using the Monte Carlo method, and in the paper[11]—with the help of a quasiequilibrium thermodynamic approach. It is worth noting, however, that in almost all these publications (with the exception of Ref. 6) the free electron concentration was assumed to be of the order of 10^{17} cm^{-3}, and in all these papers the comparison of calculated results with the experimental data was not presented. An explanation of this fact is absence of the experimental data obtained using these comparatively pure crystals. Indeed, such purity of InN crystals could not be attained by that time technologies, and in the only known to us experimental study[12] of high field transport the samples with a much higher free electron concentration of 9×10^{18} cm^{-3} were used.

In this paper the high field electron transport in InN is studied theoretically under the conditions that correspond to the experimental situation using the new parameters of the InN electron spectrum and a new numerical method for the solution of the Boltzmann transport equation.

The paper is organized as follows. In the Sec. II, we describe a physical model of the semiconductor we use in the subsequent calculations. The main results, i.e., electron drift velocity-field characteristics of InN in various conditions, are presented in the Sec. III. The results are discussed and conclusions are made in the Sec. IV. The calculation method is briefly described in the Appendix.

[a)]Electronic mail: dmitriev@lt.phys.msu.su.

II. MODEL DESCRIPTION

There is a certain disagreement in the literature about the values of InN material parameters. We could find four different sets of them (Table I). LO- and TO-phonon energies are taken from the review of electron and vibrational states of InN,[13] in which the narrow band gap value $\varepsilon_g=0.7$ eV is also recommended. Material parameters constituting S1 set were recommended in the review of the structure and electronic properties of InN,[14] and were earlier used in the paper[15] to calculate low-field electron transport properties of InN. The band gap width $\varepsilon_g=0.7$ eV was also adopted in the papers[9,10] for studies of the hot electron transport in InN. In these papers the electron effective mass in the Γ-point of the Brillouin zone was set to $m_\Gamma=0.045m_0$, m_0 being the free electron mass. The set S4 was recommended in the review article.[16] The set S3 is similar to S4, it was used in the papers[4–6,11] to calculate the drift velocity-field characteristics of InN.

In this paper, we concentrate on purely electron transport in n-InN and hence use a one-valley model to approximate the band structure of InN. The lower conduction band minimum is assumed to be in the Γ-point of the Brillouin zone. The energy dispersion relation in the neighborhood of the Γ-point is assumed to be isotropic but nonparabolic

$$\frac{\hbar^2k^2}{2m_\Gamma}=\varepsilon(1+\alpha\varepsilon), \tag{1}$$

where ε is the electron energy, $\mathbf{k}$ is the wave vector, and α is the nonparabolicity parameter that can be expressed as

$$\alpha=\frac{1}{\varepsilon_g}\left(1-\frac{m_\Gamma}{m_0}\right)^2. \tag{2}$$

The higher energy valleys in the conductivity band are not taken into account in our calculations because there is no unanimous information about their location and characteristics. However, we performed test calculations assuming that the second valley of the conductivity band is situated in the A-point of Brillouin zone with its minimum lying 2 eV above the Γ-valley minimum. In our calculations the dispersion relation in the A-band was taken isotropic and parabolic, the electron effective mass was equal to the free electron mass. Using the results of the test calculations, we study

TABLE I. Four sets, S1 to S4, of InN material parameters.

Quantity	Unit	S1	S2	S3	S4
Band gap	eV	0.7		1.9	2.0
Effective mass	m_0	0.07	0.045	0.11	0.12
High-frequency dielectric constant	⋯	6.7		8.4	
Static dielectric constant	⋯	11.0		15.3	
LA-phonon velocity	10^5 cm/s	5.2		6.24	
TA-phonon velocity	10^5 cm/s	1.2		2.55	
Acoustical deformation potential	eV	3.6		7.1	
LO-phonon energy	meV	73			
TO-phonon energy	meV	57			
Piezoelectric constant	C/m^2	0.375			
Mass density	g/cm^3	6.81			

below the electron transport in the electric field range where the intervalley scattering does not affect the results.

In our calculations all electron scattering mechanisms important in the nitride semiconductors are taken into account, i.e., ionized impurity scattering and scattering by phonons, namely, deformation and polarization acoustical and polar optical ones. In this paper, however, we do not take into account electron-electron interaction. We neglect holes in the valence band. The phonon system is assumed to be in the equilibrium and the lattice temperature does not depend upon the field and remains constant.

III. RESULTS

First, the calculations with different sets of InN material parameters (Table I) were performed under conditions similar to the experimental ones,[12] i.e., lattice temperature was 77 K and the free electron concentration 9×10^{18} cm^{-3}. The comparison of the calculated field dependence of electron drift velocity with the experimental data[12] is presented in Fig. 1. One can see that the best fit of the experimental curve is provided by the set S4, which includes the older band parameter values obtained just for heavily doped samples with electron concentration close to one used in our calculations. The results for the set S3 do not differ significantly, the slightly lighter electron effective mass resulting in a somewhat higher mobility. The results obtained for the most topical set S1 are also very close to the experimental ones. So we cannot unambiguously give preference to one of these three sets of material parameters. However, the set S2 with its very light electron effective mass provides considerably worse agreement with the experimental data.

For the further more detailed study of InN high-field electron properties, we have taken the set S1. We have chosen this set because it is more up to date and seems more reliable. The use of this set provides good fit of experimental data and, as far as we know, this set was not examined before in similar calculations.

In Figs. 2 and 3 the calculations for the material with the fixed low electron concentration $N_e=1\times10^{17}$ cm^{-3} and different charged impurity concentrations N_i in the range from 1×10^{17} to 9×10^{18} cm^{-3} are presented. The figures show that charged impurity scattering is very effective at the high impurity concentrations exceeding approximately 1×10^{18} cm^{-3} so that no manifestations of electron heating can be observed in the corresponding v_d-E curves that remain perfectly linear in the whole field interval. The influence of phonon scattering on the electron mobility is minimum here, as is evident from the comparison of the lower curves in Figs. 2 and 3 that almost coincide. The electron mobility is of the order of several hundreds of cm^2/V s.

At the lower impurity concentration $N_i=1\times10^{17}$ cm^{-3} the Ohmic mobility becomes considerably higher, especially

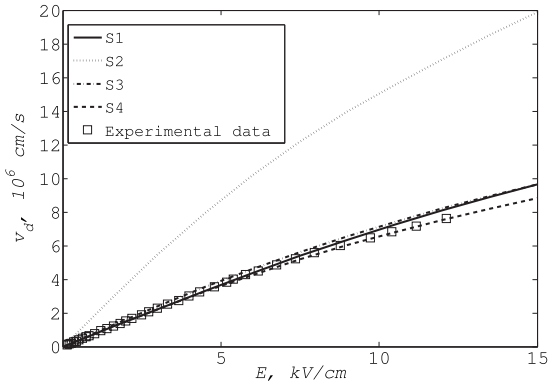

FIG. 1. The calculated field dependence of the drift velocity v_d for different sets of InN material parameters, the lattice temperature is 77 K, the free electron, and doping concentrations are 9×10^{18} cm^{-3}. Experimental data are taken from Ref. 12.

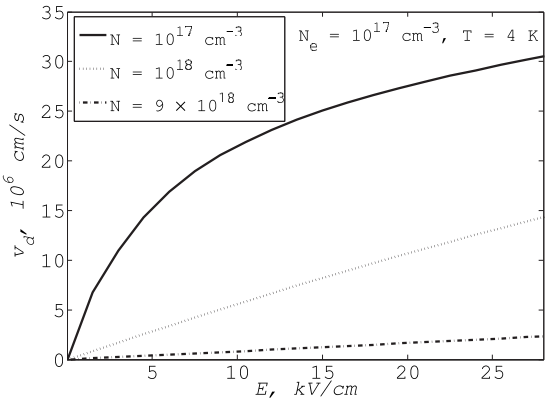

FIG. 2. The calculated field dependence of the drift velocity v_d in InN with different charged impurity concentration N_i at the lattice temperature $T=4$ K and the electron concentration $N_e=1\times10^{17}$ cm^{-3}. $N_i=1\times10^{17}$, 1×10^{18}, and 9×10^{18} cm^{-3}, parameter set S1.

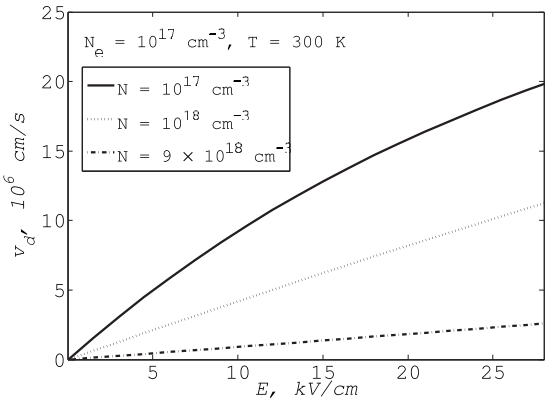

FIG. 3. The calculated field dependence of the drift velocity v_d in InN with different impurity concentration at the lattice temperature $T=300$ K and the electron concentration $N_e=1\times10^{17}$ cm^{-3}. $N_i=1\times10^{17}$, 1×10^{18}, and 9×10^{18} cm^{-3}, parameter set S1.

at 4 K where it exceeds 4×10^3 cm^2/V s. A substantial heating of the electron system takes place in these conditions, and v_d-E curves become highly nonlinear. In the high-field region the differential mobility significantly decreases (Fig. 2, upper curve). Intensive scattering of the hot electrons with energy beyond the optical phonon scattering threshold can be considered as the reason of this decrease.

At 300 K, the mean electron energy is higher, and the optical phonon scattering is intensive already in low fields, so there is no big change in scattering conditions as electrons heat up, and the mobility varies only moderately (Fig. 3, upper curve).

In Figs. 2 and 3 different levels of impurity compensation were considered. In the further calculations, we study a more common situation when the compensation is absent and hence the doping concentration N_i and free electron concentration N_e coincide.

In Fig. 4 the field dependence of InN drift velocity is presented at the lattice temperature $T=77$ K for different doping levels. The drift velocity decreases significantly with the increase in the doping level due to more intensive ionized impurity scattering. Simultaneously, the electron Fermi energy increases as N_e grows up, and this leads to more intensive optical scattering and again to the mobility reduction.

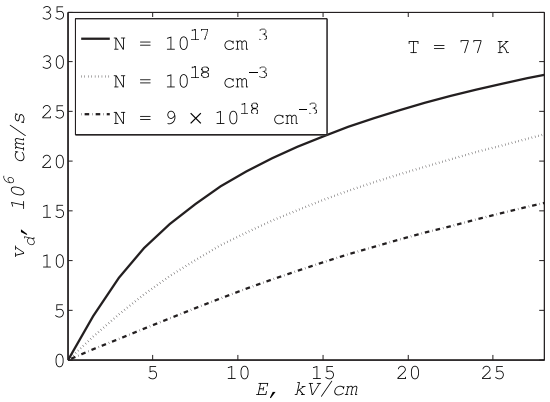

FIG. 4. The calculated field dependences of the drift velocity v_d for different doping levels. No compensation: $N=N_e=N_i$, the lattice temperature 77 K, the set S1.

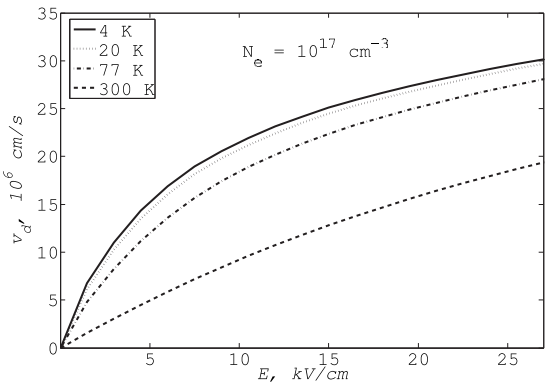

FIG. 5. The calculated field dependence of the drift velocity v_d at different lattice temperatures for the set S1 and the doping level 1×10^{17} cm^{-3}.

As in Fig. 2 above, a higher level of nonlinearity of the field-velocity curves is evident in the lightly doped samples. Intensive cooling of the hot electrons with the energy beyond the optical phonon energy can be considered as the reason, as discussed earlier.

The lattice temperature influence on InN velocity-field characteristics is illustrated in Figs. 5–7 for the free electron concentrations of 1×10^{17} cm^{-3}, 1×10^{18} cm^{-3}, and 9×10^{18} cm^{-3}. Every figure contains the curves calculated for the lattice temperature of 4, 20, 77, and 300 K. Comparing the figures, one can clearly see that the drift velocity significantly decreases with the increase in the doping level. This effect is more prominent at low temperatures when the phonon scattering is less effective but still can be clearly seen at 300 K, which indicates that impurity scattering is important at the room temperature, too. As above, nonlinearity of the field-velocity curves increases with the decrease in the free electron concentration, as illustrated by increasing difference between low-field (Ohmic) and high-field differential mobilities (Table II).

The drift velocity decreases as the lattice temperature is increased. Acoustical phonon scattering is the main reason of this fact (we checked it by turning this scattering mechanism on and off in our test calculations). Furthermore, the relative difference between the curves corresponding to different temperatures increases with the decrease in the doping level.

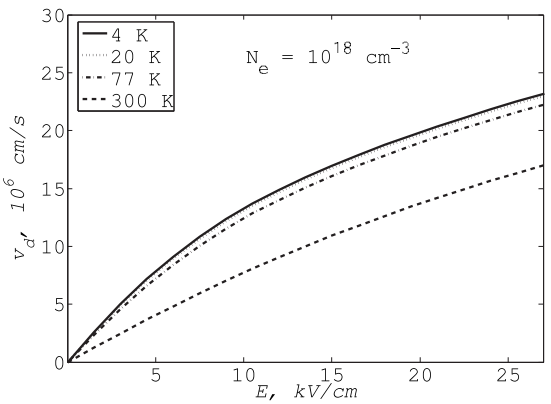

FIG. 6. The calculated field dependence of the drift velocity v_d at different lattice temperatures for the set S1 and the doping level 1×10^{18} cm^{-3}.

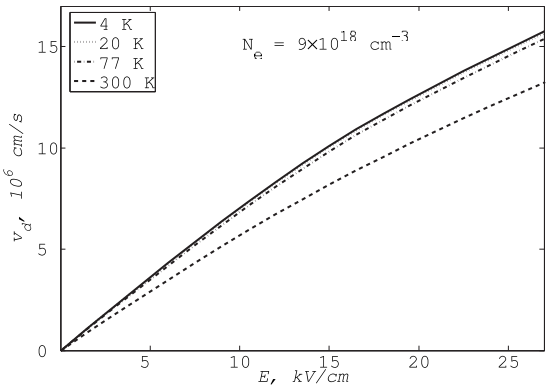

FIG. 7. The calculated field dependence of the drift velocity v_d at different lattice temperatures for the set S1 and the free electron concentration 9×10^{18} cm^{-3}.

Indeed, the relative significance of the phonon scattering compared with the ionized impurity scattering increases with the decrease in the impurity concentration.

The velocity-field characteristics of InN with the free electron concentration 9×10^{18} cm^{-3} at different lattice temperatures are presented in Fig. 7. One can clearly see that the drift velocity decreases as the lattice temperature is increased, the signature of phonon scattering. However, the effect is not very prominent, and this shows that the main electron scattering mechanism at high doping levels is interaction with charged impurities.

IV. CONCLUSION

The hot electron transport in wurtzite InN has been studied. Different sets of material parameters were examined, the results were compared with the experimental data.[12] It has been shown that the sets S1 and S4 (Table I) provide the best fit of experimental curve. The more up to date set S1 was used to study field dependence of the electron drift velocity in InN under different conditions.

ACKNOWLEDGMENTS

The work was supported by the Federal special purpose program "Scientific and teaching personnel of innovative Russia in 2009–2013" via the contract P-2312.

APPENDIX: THE NUMERICAL METHOD

To describe the electron transport in bulk InN subject to an electric field **E** we use the Boltzmann transport equation (BTE) as follows:

$$\frac{\partial f(\mathbf{k})}{\partial t} = -\frac{e\mathbf{E}}{\hbar}\frac{\partial f(\mathbf{k})}{\partial \mathbf{k}} + \widehat{St}(f),$$

here $\mathbf{k}$ denotes the electron wave vector, and the electron distribution function $f(\mathbf{k})$ satisfy the usual condition

$$\sum_{\mathbf{k}} f(\mathbf{k}) = NV,$$

where N is the free electron concentration, V is the crystal volume. The major electron scattering mechanisms are taken into account in the collision integral

$$\widehat{St}(f) = \sum_{\mathbf{k}'} \{W(\mathbf{k}' \to \mathbf{k}) f(\mathbf{k}')[1 - f(\mathbf{k})] - W(\mathbf{k} \to \mathbf{k}') f(\mathbf{k}) \times [1 - f(\mathbf{k}')]\},$$

$W(\mathbf{k} \to \mathbf{k}')$ being the electron transition rate from the state $\mathbf{k}$ into $\mathbf{k}'$. The relevant scattering mechanisms in the nitride semiconductors do not affect the spin of electron, and hence there is no summation with respect to the electron spin indices in the collision integral.

The well-established Monte Carlo approach[17] is a powerful tool for solving BTE. It makes it possible to study charge transport in a wide range of materials and physical situations with rather high accuracy. But in the case of nonlinear BTE the method becomes very time consuming,[17] because ensemble Monte Carlo study is to be performed. The complications that appear when one tries to study the electron transport in the transient regime seem to be its second significant disadvantage.[17]

Deterministic methods based on the collision integral linearization with respect to the distribution function assuming

$$f[1 - f] \simeq f,$$

and on the distribution function expansion in terms of a suitable basis function set were developed in recent years.[18,19] Thus, a linear equation set is to be solved instead of BTE. These methods are quite accurate and effective from the computational point of view but they become inappropriate when the linearization cannot be carried out, e.g., when electron gas is degenerate. It is worth noting that in InN the free electron concentration is usually rather high so that the electron gas becomes degenerate even at the room temperature.

In this paper, we apply a new iterative method that requires only the smoothness of the distribution function. With the help of this method, one can find the stationary distribution function as well as its time evolution.

TABLE II. Low-field (left) and high-field (right) differential mobilities in cm^2/V s for different lattice temperatures and doping levels (no compensation: $N_e = N_i$).

	4 K		20 K		77 K		300 K	
10^{17} cm^{-3}	4491	330	4082	340	3189	367	1026	452
10^{18} cm^{-3}	1721	429	1680	428	1554	427	823	431
9×10^{18} cm^{-3}	729	415	724	414	705	408	587	376

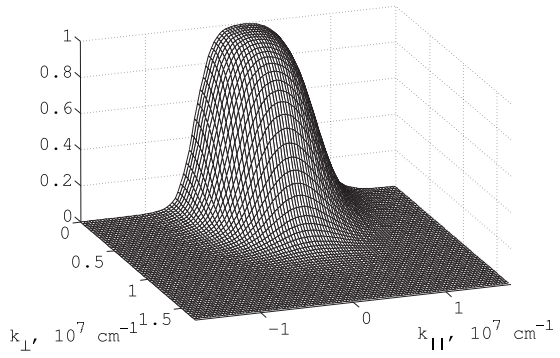

FIG. 8. The electron distribution function calculated for $E=30$ kV/cm, $T=77$ K, $N=9\times10^{18}$ cm^{-3}, and S1 parameter set. Grid size is 15×30, time increment $\Delta t=10^{-15}$ s, simulation time $t_{sim}=0.5\times10^{-12}$ s. One can see that the field shifts the distribution function along $k_{\|}$ axis.

Basics of the method are as follows. If the electron spectrum can be considered isotropic, BTE can be modified taking into account an axial symmetry of the distribution function:

$$f(\mathbf{k}) = f(k_{\|},k_{\perp}),$$

where $k_{\|}$ and $k_{\perp}$ are the momentum components parallel and perpendicular to the applied field, correspondingly. So the problem becomes a two-dimensional one. Now we introduce a square grid on the momentum plane:

$$k_{\|}^{i} = -k_{\max} + (i+1/2)\Delta_0, \quad i = 0,1,\ldots,\frac{2k_{\max}}{\Delta_0} - 1,$$

$$k_{\perp}^{j} = j\Delta_0, \quad j = 0,1,\ldots,\frac{k_{\max}}{\Delta_0},$$

the distribution function values at the grid nodes are unknowns to be found. The grid can be sparse if the distribution function is expected to be smooth. The size of the simulation area, $k_{\max}$, should be chosen so that the distribution function remains well localized within the simulation area. This means that, on the one hand, $k_{\max}$ should be large enough but on the other hand, the computational complexity increases for large $k_{\max}$, so it should not be taken greater than required. As the distribution function itself, $k_{\max}$ depends on the applied field strength.

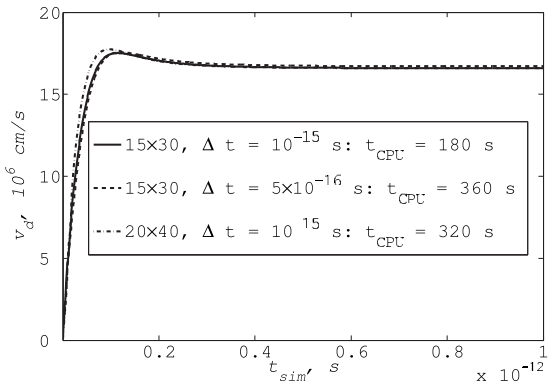

FIG. 9. The illustration of the convergence. The dependence of the drift velocity v_d on calculation time, $E=30$ kV/cm, $T=77$ K, $N=9\times10^{18}$, S1 set.

At the initial moment of time, $t=0$, the electron distribution function in the grid nodes is approximated by an equilibrium Fermi distribution function. Then the iterations begin, and the $(n+1)$th iteration step is organized in the following way. The distribution function $f^n(k_{\|},k_{\perp})$, found at the preceding nth step, is used to calculate the collision integral values. The distribution function values in intermediate $(k_{\|},k_{\perp})$-points, which are necessary for numerical integrations in the collision integral, can be interpolated from the grid nodes in the $(k_{\|},k_{\perp})$-space using the bicubic spline interpolation.[20] Note that the collision integral values are to be calculated on the grid nodes only, thus we have $\widehat{St}_{ij}$. Now the new distribution function values in the grid nodes are evaluated according to BTE

$$f_{ij}^{n+1} = f^n\left(k_{\|} - \frac{eE}{\hbar}\Delta t, k_{\perp}\right) + \Delta t\widehat{St}_{ij},$$

where Δt being a time step (its choice is discussed below). This iterative procedure can be considered as the time evolution of the distribution function according to BTE. The iterations are continued until the convergence is obtained.

In our calculations, the simulation area size $k_{\max}$ was taken equal to 1.7×10^7 cm^{-1}. Figure 8 shows that the distribution function is localized within the simulation area.

The convergence of the method was verified in test runs. Figure 9 illustrates the time dependence of the drift velocity for different parameters of the numerical method. Unfortunately, it is difficult to find an easy way to show the convergence of the distribution function itself because of the three-dimensional nature of the corresponding graphs. For the fixed field value $E=30$ kV/cm, electron concentration $N=9\times10^{18}$ cm^{-3}, and lattice temperature $T=77$ K, different time steps Δt and grid sizes were examined. We found $\Delta t=10^{-15}$ s and the grid size 15×30 to be optimum for the current task. Figure 9 shows that a decrease of Δt and an increase in the grid size do not affect the result.

The authors consider the method described above as a convenient tool for the study of similar electron transport problems in semiconductors. The method can be used under different conditions, including the degenerate electron gas statistics. There is no fitting parameters, all relevant scattering mechanisms can be easily taken into account. The method can be also used to study the charge transport in the transient regime. Furthermore, it is quite computationally effective.

[1]V. Yu. Davydov, A. A. Klochikhin, R. P. Seisyan, V. V. Emtsev, S. V. Ivanov, F. Bechstedt, J. Furthmüller, H. Harima, A. V. Mudryi, J. Aderhold, O. Semchinova, and J. Graul, Phys. Status Solidi B **229**, R1 (2002).
[2]V. Yu. Davydov, A. A. Klochikhin, V. V. Emtsev, S. V. Ivanov, V. V. Vekshin, F. Bechstedt, J. Furthmlüler, H. Harima, A. V. Mudryi, A. Hashimoto, A. Yamamoto, J. Aderhold, J. Graul, and E. E. Haller, Phys. Status Solidi B **230**, R4 (2002).
[3]C. J. Humphreys, MRS Bull. **33**, 459 (2008).
[4]E. Bellotti, B. K. Doshi, K. F. Brennan, J. D. Albrecht, and P. P. Ruden, J. Appl. Phys. **85**, 916 (1999).
[5]B. E. Foutz, S. K. O'Leary, M. S. Shur, and L. F. Eastman, J. Appl. Phys. **85**, 7727 (1999).
[6]S. K. O'Leary, B. E. Foutz, M. S. Shur, and L. F. Eastman, J. Appl. Phys. **83**, 826 (1998).
[7]S. K. O'Leary, B. E. Foutz, M. S. Shur, and L. F. Eastman, Appl. Phys.

Lett. **87**, 222103 (2005).
[8]E. Starikov, P. Shiktorov, V. Gruinskis, L. Varani, J. C. Vaissière, C. Palermo, and L. Reggiani, J. Appl. Phys. **98**, 083701 (2005).
[9]V. M. Polyakov and F. Schwierz, Appl. Phys. Lett. **88**, 032101 (2006).
[10]V. M. Polyakov and F. Schwierz, J. Appl. Phys. **99**, 113705 (2006).
[11]C. G. Rodrigues, A. R. Vasconcellos, R. Luzzi, and V. N. Freire, J. Appl. Phys. **98**, 043702 (2005).
[12]D. Zanato, N. Balkan, B. K. Ridley, G. Hill, and W. J. Shaff, Semicond. Sci. Technol. **19**, 1024 (2004).
[13]V. Yu. Davydov and A. A. Klochikhin, Semiconductors **38**, 861 (2004).
[14]W. Walukiewicz, J. W. Ager III, K. M. Yu, Z. Liliental-Weber, J. Wu, S. X. Li, R. E. Jones, and J. D. Denlinger, J. Phys. D **39**, R83 (2006).
[15]L. Hsu, R. E. Jones, S. X. Li, K. M. Kim, and W. Walukiewicz, J. Appl. Phys. **102**, 073705 (2007).
[16]I. Vurgaftman, J. R. Meyer, and L. R. Ram-Mohan, J. Appl. Phys. **89**, 5815 (2001).
[17]C. Jacoboni and L. Reggiani, Rev. Mod. Phys. **55**, 645 (1983).
[18]C. Ertler and F. Schruerrer, J. Phys. A **36**, 8759 (2003).
[19]M. Galler and F. Schruerrer, J. Phys. A **37**, 1479 (2004).
[20]R. Keys, IEEE Trans. Acoust., Speech, Signal Process. **29**, 1153 (1981).